Title page

Sonic hedgehog medulloblastoma cells in co-culture with cerebellar organoids converge towards *in vivo* malignant cell states

Max J. van Essen[1,2], Alina Nicheperovich[3], Benjamin Schuster-Böckler[3,4], Esther B. E. Becker[1,2] and John Jacob[1*]

[1]Nuffield Department of Clinical Neurosciences, University of Oxford, Oxford, OX3 9DU, United Kingdom

[2]Kavli Institute for Nanoscience Discovery, University of Oxford, Oxford, OX1 3QU, United Kingdom

[3]Ludwig Institute for Cancer Research, University of Oxford, Nuffield Department of Medicine Old Road Campus Research Building, Roosevelt Drive, Oxford OX3 7DQ, United Kingdom

[4]Big Data Institute, University of Oxford, Li Ka Shing Centre for Health Information and Discovery, Old Road Campus, Oxford OX3 7LF, United Kingdom

*Correspondence: john.jacob@ndcn.ox.ac.uk

Abstract

Background

In the malignant brain tumour sonic hedgehog medulloblastoma (SHH-MB) the properties of cancer cells are influenced by their microenvironment, but the nature of those effects and the phenotypic consequences for the tumour are poorly understood. The aim of this study was to identify phenotypic properties of SHH-MB cells that were driven by the non-malignant tumour microenvironment.

Methods

Human induced pluripotent cells (iPSC) were differentiated to cerebellar organoids to simulate the non-malignant tumour microenvironment. Tumour spheroids were generated from two distinct, long-established SHH-MB cell lines which were co-cultured with cerebellar organoids. We profiled the cellular transcriptomes of malignant and non-malignant cells by performing droplet-based single-cell RNA-sequencing (scRNA-seq). The transcriptional profiles of tumour cells in co-culture were compared with those of malignant cells cultured in isolation and with public SHH-MB datasets of patient tumours and patient-derived xenograft (PDX) models.

Results

SHH-MB cell lines in organoid co-culture adopted patient tumour-associated phenotypes and showed increased heterogeneity compared to monocultures. Sub-populations of co-cultured SHH-MB cells activated a key marker of differentiating granule cells, *NEUROD1* that was not observed in tumour monocultures. Other sub-populations expressed transcriptional determinants consistent with a cancer stem cell (CSC)-like state that resembled cell states identified *in vivo*.

Conclusion

For SHH-MB cell lines in co-culture, there was a convergence of malignant cell states towards patterns of heterogeneity in patient tumours and PDX models implying these states were non-cell autonomously induced by the microenvironment. Therefore, we have generated an advanced, novel *in vitro* model of SHH-MB with potential translational applications.

49

50 **Introduction**

51 Medulloblastoma (MB), a heterogeneous cerebellar tumour consisting of four major
52 subtypes is the commonest malignant brain tumour of childhood, [1] of which nearly a third
53 are classed as Sonic Hedgehog medulloblastoma (SHH-MB).[2] During development, SHH
54 acting as a mitogen promotes massive expansion of the upper rhombic lip-derived
55 cerebellar granule cell population in the external granule layer (EGL).[3] Somatic or germ-line
56 mutations and focal somatic copy number alterations in SHH pathway tumour suppressors
57 or oncogenes are the commonest events leading to aberrant SHH pathway activation and
58 tumorigenesis in granule progenitors.[2] High-risk variants of SHH-MB still carry a dismal
59 prognosis, which emphasises the importance of gaining a greater understanding of how
60 tumours progress so that improved therapies can be developed.

61

62 In patients and mouse models, SHH-MB contains SOX2^{+} tumour-propagating neural stem-
63 like cells, equivalent to cancer stem cells (CSC) and more differentiated cells.[2] By hijacking
64 mechanisms of self-renewal in neural stem cells (NSC) and pluripotent stem cells, CSC can
65 replenish tumours in transplantation assays.[4] During mammalian neurogenesis, initial
66 ubiquitous SOX2 expression in the early embryonic central nervous system attenuates as
67 the balance shifts from self-renewal to differentiation.[5] By contrast, in SHH-MB persistent
68 SOX2-expressing granule progenitor-derived CSC can reconstitute tumours after therapy
69 and support a hierarchical model of tumorigenesis.[6] Furthermore, cross-talk between the
70 microenvironment and other brain tumour types suggests that cell extrinsic factors could
71 also influence malignant cell states.[4] However, the complexity of the *in vivo* tumour
72 microenvironment poses a challenge in discerning the involvement of distinct non-
73 malignant components.

74

75 To address how the microenvironment affects tumour progression, we sought to evaluate
76 the phenotypes of SHH-MB cells using single-cell transcriptomics, under defined conditions
77 that we anticipated might simulate *in vivo* tumour growth. To this end we leveraged
78 cerebellar organoid differentiation from human induced pluripotent stem cells (hiPSC)
79 through their co-culture with two SHH-MB cell lines [7] that were compared with conventional
80 *in vitro* tumour monocultures. Organoids can be grown in xeno-free culture medium and

81 they contain defined neuronal and glial cell types. Although lacking immune cells or blood
82 vessels, they provide more physiological conditions than conventional *in vitro* models
83 enabling the evaluation of tumour cell phenotypes in a simulated native
84 microenvironment.[8]
85
86 **Materials and Methods**
87 Organoid differentiation
88 Cerebellar organoid differentiation was performed as described previously.[9] In brief, human
89 iPSC line AH017-3 cells [10] were detached by incubation with pre-warmed TrypLE for 5
90 minutes. Cells were collected by centrifugation and resuspended in induction medium (50%
91 IMDM, 50% F12, 7ug/mL Insulin, 5mg/mL BSA, 1X Chemically defined Lipid concentrate,
92 450uM Monothioglycerol, 15ug/mL Apo-transferrin, 1X Penicillin/Streptomycin) at a final
93 concentration of 100,000 cells/ml. 10,000 cells per well were plated in an ultra-low-
94 attachment V-bottom 96 well plate and returned to the incubator. After two days, FGF2 was
95 added at a final concentration of 50 ng/ml. One-third medium change was performed at day
96 7 and full medium change at day 14. On this day, the organoids were also transferred into a
97 low-attachment 48-well plate. On day 21, medium was changed to differentiation medium
98 (Neurobasal + 1% N2 supplement + 1% GlutaMAX + 1X Penicillin/Streptomycin) and
99 subsequent full medium changes were performed on days 28 and 35. After day 35, medium
100 was changed twice/week.
101
102 Medulloblastoma cell lines, tumour spheroids and organoid-tumour spheroid co-culture
103 DAOY-GFP cells (gift from Vincenzo D'Angiolella, DAOY cell line originally purchased from
104 ATCC) were grown in monolayer culture in MEM, 1% GlutaMAX, 1X Penicillin/Streptomycin
105 and 1% FBS (cell line authentication in Supplementary Table 1). ONS-76-Luciferase-GFP cells
106 (gift from Louis Chesler; ONS-76 cell line originally purchased from JCRB Cell Bank by Steven
107 Clifford) were grown in monolayer culture in RPMI + 1% GlutaMAX + 1X
108 Penicillin/Streptomycin + 1% FBS (Supplementary Table 1). Medium was changed twice per
109 week. To generate tumour spheroids, cells were detached by incubation with pre-warmed
110 TrypLE for 5 minutes and collected by centrifugation. Cells were resuspended in
111 differentiation medium at a concentration of 200,000 cells/ml and plated in an ultra-low-
112 attachment V-bottom 96-well plate at 20,000 cells per well. In preparation for cerebellar

113 organoid-tumour spheroid co-culture, one week prior to the start of co-culture, tumour
114 spheroids were generated as described above. One tumour spheroid was placed with one
115 day 35 organoid in a low-attachment 24-well plate in identical differentiation medium. The
116 size ratio of the organoid to the tumour spheroid of approximately five-to-one ensured that
117 the organoid microenvironment could encompass the tumour spheroid to facilitate their
118 interaction. To allow fusion of the tumour spheroid and the organoid, the plate was
119 incubated for two days at a 45-degree angle. Medium was changed twice per week and the
120 cells were maintained in co-culture, alongside tumour spheroid and tumour monolayer
121 cultures for a further 25 days (Fig. 1A).
122
123 Single cell isolation
124 Day 60 organoids and organoid-tumour co-culture samples were collected using a wide bore
125 pipette tip and placed in a 6-well plate. Five tumour spheroid-organoid co-cultures for each
126 cell line and a similar number of control organoids were each cut in four pieces and placed
127 in an Eppendorf tube. After removal of excess medium, 200 µl of pre-warmed (to 37°C)
128 Neuron isolation enzyme was added and the tube was placed in a 37°C water bath.
129 Organoids were incubated with the enzyme for 30 minutes with intermittent agitation. The
130 enzyme was removed and organoids were washed once with HHGN medium (HBSS + 2.5mM
131 HEPES + 35mM Glucose + 4mM $NaHCO_3$). Organoids were then dissociated in differentiation
132 medium by gentle trituration. Afterwards, the cell suspension was enriched for viable cells
133 using the dead cell removal kit (Miltenyi Biotec) following the manufacturers protocol. Cell
134 viability was determined using Trypan Blue staining and counted using an automated cell
135 counter (Applied Biosystems Countess 3). Cells were centrifuged at 300 x *g* for 5 minutes
136 and resuspended in the appropriate volume of resuspension buffer (HBSS + 0.04% BSA) to a
137 final concentration of 2000 cells/µl before proceeding with single-cell RNA sequencing.
138 Thirty tumour spheroids were collected using a wide bore pipette tip and placed in an
139 Eppendorf tube. Excess medium was removed and 200 µl of pre-warmed Neuron isolation
140 enzyme (Gibco) was added. The tube was placed in a 37°C water bath for 20 minutes and
141 agitated every 5 minutes. Subsequent processing was performed following the same steps
142 as described above. DAOY and ONS-76 cell monolayer cultures were dissociated by
143 incubation with pre-warmed TrypLE for 5 minutes. TrypLE was then diluted in PBS before

144 centrifugation at 400 x *g* for 5 minutes to collect the cells. Cells were washed once in
145 differentiation medium before processing as described above. Single cell barcoding and
146 reverse transcription of poly-A mRNA was performed using the 10X Chromium controller (3'
147 version 3.1 chemistry) and sequencing of single-cell libraries was performed on an Illumina
148 NovaSeq6000 sequencing system according to the manufacturer's instructions.
149
150 Data pre-processing and analysis
151 Initial sequencing data exploration was performed using Cell Ranger v6.1.1. For each dataset
152 we removed cells with 10% or higher mitochondrial gene expression [11] and genes expressed
153 in fewer than 10 cells. Sequencing confirmed the greater proportion of non-malignant to
154 malignant cell types in co-culture which was expected given the relative sizes of the
155 organoid and tumour spheroid (Supplementary Table 2). Downstream analysis largely
156 implemented the workflow of Seurat v4, which is robust to limited cell numbers.[12] We used
157 the 'sctransform' modelling framework, which corrects counts for each gene in a cell by
158 regressing out sequencing depth.[13] The difference between G2M and S phase scores was
159 regressed out so that differences in cell cycle phase among proliferating cells was
160 eliminated, while at the same time retaining signals separating cycling and non-cycling cells.
161 For differential gene expression testing between clusters a Bonferroni-corrected p-value <
162 0.05 was considered significant. To perform gene set enrichment analysis, we first used the
163 R package PRESTO which performs a fast Wilcoxon rank sum test on the Seurat clusters.[14]
164 We then tested functional enrichment of Seurat clusters of interest using gene sets from
165 MsigDB and the fgsea package.[15,16] Visualisation of pathway enrichment analysis was
166 performed using g:Profiler to search for Gene Ontology pathways that were significantly
167 enriched in a gene list before visualising the results using EnrichmentMap in Cytoscape.[17,18]
168 Pathway gene sets with fewer than three genes and more than 350 genes were excluded in
169 line with the default g:Profiler and Cytoscape workflows. For g:Profiler, a Benjamini-
170 Hochberg false discovery rate adjusted p-value of < 0.05 was considered significant.
171 Pseudotime analysis was conducted using Monocle 3.[19] Dataset integrations were, in
172 general, performed using standard workflows in Seurat v4, except when integrating
173 malignant cell populations (see Fig. 5) where we observed strong blending of distinct
174 malignant cell states. Instead, we used the fastMNN algorithm,[20] which was found to

175 preserve biological differences between cancer cell populations, while ensuring effective
176 batch correction.[21]
177 Statistical Analysis
178 Statistical significance testing was performed using R.
179
180 **Results**
181 We co-cultured malignant tumour spheroids of ONS-76 cells or DAOY cells, which harbour
182 wild type and mutant copies of *TP53*, respectively with non-malignant cerebellar organoids
183 differentiated from human iPSC (Fig. 1A; Supplementary Fig. S1A). As controls, tumour cells
184 were grown as monolayers or tumour spheroids while non-malignant organoids were grown
185 separately. These long-established cell lines were chosen because of their evolutionary
186 divergence from patient tumours. Our approach was designed to enhance the detection of
187 malignant cell states induced by the non-malignant microenvironment, when comparing
188 monocultures to the co-culture conditions. Using primary SHH-MB or PDX cultured cells
189 could potentially mask such differences, given their closer resemblance to *in vivo* cell states,
190 thus obscuring microenvironmental impacts on tumour cell properties. After 25 days in co-
191 culture, cells were dissociated and processed for single-cell RNA sequencing (scRNA-seq) on
192 the 10X Chromium platform. After filtering the dataset in accordance with our quality
193 control thresholds we selected 13,534 cells for further analysis (Supplementary Fig. S1B – E;
194 Supplementary Table 2). We used Seurat to visualise the relationship between samples by
195 clustering and projected cells in a common UMAP space labelled according to their sample
196 of origin (Supplementary Fig. S1F, G). ONS-76 cells and DAOY cells cultured as monolayers or
197 tumour spheroids formed well-demarcated clusters. In contrast, there was extensive
198 overlap of co-cultured cells with the non-malignant organoid control, which was anticipated
199 given the large numbers of cells recovered belonging to organoid cellular subtypes. Only a
200 handful of cells from the non-malignant control organoid clustered with the exclusively
201 malignant samples, confirming that the clustering reflected biological differences between
202 the samples. In the co-cultured samples, several times the number of cells clustered with
203 the malignant samples suggesting the latter cells were malignant cells in co-culture.
204
205 **ONS-76 and DAOY cells cultured as monolayers or tumour spheroids were enriched for**
206 **proliferative, protein biosynthetic and wound healing processes**

207 We performed an integrated analysis of ONS-76 monolayer and tumour spheroid
208 transcriptomes in Seurat [13] and compared the transcriptional programmes of malignant cells
209 using functional enrichment analysis in the two conditions.[16] ONS-76 cells grown as
210 monolayers were enriched for Gene Ontology (GO) terms for cell cycle associated genes
211 (Supplementary Fig. S2A and Supplementary Table 3). In comparison, genes upregulated in
212 tumour spheroids were associated with altered cell morphology and wound healing for
213 example *IFITM3, IGFBP2, IGFBP5, STC1* and *SPARC* (Supplementary Fig. S2B – C and
214 Supplementary Table 3) consistent with an epithelial-to-mesenchymal transition (EMT) state
215 and tumour stroma production.[22] Upon clustering of the ONS-76 tumour spheroid sample
216 (Supplementary Fig. S2D), expression of these genes was distributed over all clusters
217 (Supplementary Fig. S2E) supporting relative homogeneity of malignant cell states with
218 mostly arbitrary distinctions between clusters, with two exceptions. The first consisted of a
219 cluster of cycling cells, denoted 'cluster 4' that was marked by the expression of genes
220 including *MKI67*, *MYBL2*, *BIRC5* and *RRM2* consistent with a proliferative cell state
221 (Supplementary Fig. S2D, G). Although the same genes were expressed in the ONS-76
222 monolayer sample, they were not restricted to a single cluster (Supplementary Fig. S2I). A
223 second ONS-76 tumour spheroid cluster, 'cluster 0' expressed ribosomal genes and was
224 enriched for protein synthesis pathways (Supplementary Fig. S2D and Supplementary Table
225 4), which is a feature common to many cancers.[23] Less heterogeneity was evident in ONS-76
226 cells cultured as monolayers, which could be split into two clusters also distinguished by
227 their relative enrichment for ribosomal genes and protein synthesis (Supplementary Fig.
228 S2H; Supplementary Table 4). In comparison to ONS-76 tumour spheroids, expression of
229 proliferation genes spanned both clusters, although the proliferation signal of individual
230 cells was weaker (Supplementary Fig. S2H, lower panel).
231
232 Broadly similar findings were observed upon analysis of DAOY cells cultured as monolayers
233 and tumour spheroids. An integrated analysis of the cellular transcriptomes revealed
234 protein synthesis gene sets as the only significant enrichment (Supplementary Table 5) in
235 DAOY tumour spheroids. In common with ONS-76 cells, wound healing gene sets were also
236 upregulated, but in DAOY monolayers rather than in DAOY tumour spheroids. Furthermore,
237 there was a degree of enrichment in oncogenic signature gene sets that was statistically

238 non-significant for transcriptional responses of cerebellar granule progenitors to activation
239 by SHH, which acts as a mitogen for these cells (Supplementary Table 5).
240
241 Clustering of the DAOY tumour spheroid sample also revealed enrichment of protein
242 synthesis and cell cycle related pathways, respectively in two out of five DAOY tumour
243 spheroid clusters (Supplementary Fig. S2F; Supplementary Table 5). Therefore, in tumour
244 spheroids of both cell lines, those cells with a signature of enhanced proliferation were
245 restricted to specific clusters in UMAP space, suggesting an association with a distinct cell
246 state related to malignant cell proliferation. By contrast, DAOY monolayer cells that
247 expressed a proliferative signature were spread diffusely across multiple clusters in common
248 with ONS-76 monolayer cultured cells (Supplementary Fig. S2J). Although DAOY monolayer
249 cells formed more clusters than ONS-76 cells (six in DAOY monolayers compared to two in
250 the corresponding ONS-76 sample), only three out of six of the former clusters displayed
251 significant gene set enrichment. Of these, two clusters were enriched for protein synthesis
252 pathways and the remaining cluster was only significantly enriched for cell adhesion-related
253 gene sets, which is a hallmark of cancer (Supplementary Table 5).[24] Assessment of the
254 maturity of malignant cells from tumour spheroid and monolayer samples of both cell lines
255 revealed they expressed the granule cell markers, *MEIS1,*[25] *MEIS2* [26] and *JKAMP* [27]
256 (Supplementary Fig. S2K). However, *CNTN1* which marks differentiating granule cells [28] was
257 selectively expressed only in ONS-76 samples, suggesting the maturation of DAOY cells was
258 relatively impaired (Supplementary Fig. S2K).
259
260 **ONS-76 cells in co-culture, but not in monolayers or tumour spheroids expressed**
261 ***NEUROD1***
262 To determine whether malignant cells grown in a non-malignant organoid
263 microenvironment led to altered tumour cell phenotypes, we clustered the ONS-76 sample
264 in co-culture and plotted the UMAP projection, comparing the clusters obtained with those
265 in the non-malignant control organoid (Fig. 1B; Supplementary Fig. S3A). The manual
266 annotations of non-malignant cells were highly similar to our earlier annotations of day 90
267 organoids.[29] None of the clusters of malignant cells in co-culture were identified as having a
268 match in the control organoid.
269

270 In the control organoid, granule neurons could be defined by their co-expression of
271 *NEUROD1*, *RTN1* and *RBFOX3* (Fig. 1C).[27] In the co-culture condition also, a cluster of cells
272 co-expressing these genes could be identified consistent with non-malignant granule
273 neurons (Fig. 1D). Additionally, a distinct cell cluster located adjacent to non-malignant
274 granule neurons in UMAP space could be distinguished from the latter cells by their
275 expression of *NEUROD1* only, which we labelled 'ONS76_cluster_3' (Fig. 1D; Supplementary
276 Fig. S3B; Supplementary Table 6). Furthermore, upon computational integration of ONS-76
277 samples malignant *NEUROD1*$^{+}$ cells were absent in ONS-76 monolayers and tumour
278 spheroids (Fig. 1E) and only very few were present in the DAOY samples (Fig. 1E, F).
279
280 Although *NEUROD1* marks post-mitotic granule neurons in mouse,[30] in humans this gene is
281 also expressed in cycling granule progenitors.[31] Gene set enrichment analysis of
282 'ONS76_cluster_3' revealed GO terms associated with cycling cells (Fig. 1G; Supplementary
283 Fig. S3C). By contrast, the cluster annotated as 'Granule neurons' in the non-malignant
284 organoid in co-culture and in the control organoid were enriched for terms associated with
285 differentiated neurons (Fig. 1I; Supplementary Fig. S3E, F). To validate these findings, we
286 computationally examined the cell cycle phase associated with *NEUROD1* expression in non-
287 malignant and malignant cells.[13] In the cluster annotated as 'Granule neurons' in the control
288 organoid (Fig. 1C), the fraction of *NEUROD1*$^{+}$ cells that were in G1 phase was 0.60, in G2/M
289 phase the fraction was 0.17 and the S phase fraction was 0.23. However, in ONS-76 cells in
290 co-culture the fraction of *NEUROD1*$^{+}$ cells in 'ONS76_cluster_3' in G1 phase was smaller
291 (0.38), and the fraction of cells in G2/M and S phases was higher (0.30 and 0.32,
292 respectively; $p = 5.925 \times 10^{-12}$ Chi-squared test). Therefore, ONS-76 cells activated
293 *NEUROD1,* a key molecular determinant of granule cell identity only when embedded in a
294 more physiological microenvironment, but its expression was less tightly coupled to other
295 cellular processes that imparted a differentiated neuronal identity. By comparison, analysis
296 of patient SHH-MB scRNA-seq public datasets showed that they also expressed *NEUROD1*
297 (Supplementary Fig. 4A-E) [32,33] and that for one of the datasets [32] most of these cells were in
298 G1 phase (range 0.59 – 0.69). Consistent with maturation of malignant cells, patient
299 tumours also expressed *RBFOX3* and *RTN1* (Supplementary Fig. S4A-E). Given the absence of
300 *NEUROD1* upregulation in DAOY cells in co-culture, we analysed its expression in two *TP53*
301 mutant SHH-MB in a second public MB scRNA-seq dataset to test for an association

302 between presence of the mutation and *NEUROD1* expression *in vivo*.[33] The tumours varied
303 widely in their expression of *NEUROD1* displaying both elevated and minimal expression
304 (Supplementary Fig. S4D). Therefore, absence of *NEUROD1* expression in *TP53* mutant DAOY
305 cells in tumour spheroid-organoid co-culture was not inconsistent with *in vivo* findings.
306
307 A second, smaller cluster of ONS-76 tumour cells in co-culture, 'ONS76_cluster_10' was
308 identified by differential upregulation of *HOXB2* and *POU3F2*, in common with multiple non-
309 CNS cancers including leukaemia, lung and breast cancer (Fig. 1H; Supplementary Table
310 6).[34,35] Cells in this cluster also expressed *MEIS1*, which is expressed by differentiating
311 granule cells [36] and *HOXB-AS1*, which is a member of a large family of non-coding transcripts
312 that are abnormally expressed in a wide range of cancers.[37] Consistent with the expression
313 of *MEIS1*, gene set enrichment analysis suggested this cluster contained mature cells
314 (Supplementary Fig. S3G, H). Overall, subpopulations of malignant cells expressed *in vivo*
315 markers of differentiation when they were surrounded by the more physiologic
316 microenvironment of the organoid.
317
318 **A sub-population of DAOY cells in co-culture expressed multiple cancer stem cell-like**
319 **markers**
320 The analysis of the DAOY tumour spheroid-organoid co-culture sample resulted in clustering
321 of DAOY tumour cells into three distinct groups in UMAP space designated as
322 'DAOY_cluster_9', 'DAOY_cluster_13', and 'DAOY_cluster_14' (Fig. 2A). Highly distinctive,
323 differential expression of specific markers of these putative malignant clusters was apparent
324 exemplified by *PTCH1, MEIS1, POU3F4, FGFBP3, TWIST1* and *LHX9* that displayed low or no
325 expression in non-malignant cells in co-culture and in the control organoid (Fig. 2B, D and
326 Supplementary Table 6). Noting that *POU3F4* and *FGFBP3* have been linked to a neural stem
327 cell (NSC) identity,[38,39] we compared DAOY cells in co-culture with the DAOY tumour
328 spheroid sample for expression of NSC markers (Supplementary Fig. S5A). Multiple NSC
329 markers were upregulated in DAOY cells in co-culture including *SOX2*, *NES*, *FABP7* and *MSI1*
330 (Fig. 2C). A similar trend was observed for ONS-76 cells in the three conditions, although the
331 upregulation of these NSC markers in ONS-76 cells in co-culture was not as great (Fig. 2E).
332

333 The upregulation of NSC markers in malignant cells in our co-culture model is reminiscent of
334 mouse models of SHH-MB, in which persistent SOX2-expressing granule cells designated as
335 cancer stem cells (CSC) drive tumour formation and relapse.[6,40] We therefore focused our
336 analysis on further characterising the transcriptional profile of these cells. More granular
337 analysis at the level of individual malignant clusters revealed striking differences in the
338 expression of factors known to regulate *SOX2* compared to DAOY cells cultured in other
339 conditions and ONS-76 cells (Fig. 3A).[41] Only a single DAOY cluster in co-culture,
340 'DAOY_cluster_9' expressed multiple members of the *SOX2* regulatory network consisting of
341 *POU3F2*, *ZIC2*, *OTX2*, *GLI2* and *SOX2* itself (Fig. 3B). This combinatorial pattern of gene
342 expression was not observed in ONS-76 cells in co-culture (Fig. 3C), nor in tumour spheroid
343 or monolayer samples of either cell line (Fig. 3D), or in non-malignant organoid cells (Fig.
344 3E). The co-expression of these markers in subpopulations of DAOY cells in co-culture
345 suggested these cells adopted a new cell state in the presence of a non-malignant
346 microenvironment.
347
348 We hypothesised there could be an ontological relationship between the distinct DAOY cell
349 states identified in co-culture. In particular, the UMAP plot of DAOY cells in co-culture (Fig.
350 2A) suggested 'DAOY_cluster_9' and 'DAOY_cluster_13' cells occupied opposite ends of a
351 single trajectory. A pseudotime analysis supported the notion that 'DAOY_cluster_9' could
352 undergo a progressive transition to a 'DAOY_cluster_13' cell state (Fig. 3F). Pathway
353 enrichment analysis was consistent with the pseudotime analysis and showed that
354 'DAOY_cluster_9' cells were enriched for GO terms associated with a proliferative state (Fig.
355 3G; Supplementary Table 7), whereas 'DAOY_cluster_13' was enriched for neuronal
356 differentiation terms (Fig. 3H and Supplementary Table 7). The last cluster,
357 'DAOY_cluster_14' was transcriptionally less similar to the other DAOY clusters (Fig. 2A).
358 Enriched pathways for this cluster related to Notch and Hedgehog signalling, translation
359 regulation and included extracellular matrix composition and wound healing gene sets in
360 common with tumour cells cultured in isolation (Fig. 3I; Supplementary Table 7).
361
362 **CSC-like cells with a molecular profile resembling DAOY tumour cells in co-culture are**
363 **present in patient SHH-MB**

364 We analysed the expression of the *SOX2* regulatory network in a public scRNA-seq dataset
365 of patient SHH-MB.[32] Upon clustering tumour cells in Seurat [13] a single cluster in one of
366 three SHH-MB tumours expressed a highly similar network in which *OTX2* was replaced by
367 expression of another member of the regulatory network, *SRRT* (Fig. 3A and Fig. 4A).[41]
368 Furthermore, in one of two PDX models of SHH-MB from the same dataset,[32] a single
369 cluster expressed a common network, consisting of *POU3F2*, *OTX2*, *SRRT*, *GLI2* and *SOX2*
370 (Fig. 4A). Given these differences, and to determine the prevalence and identity of cells
371 expressing a signature of a *SOX2* regulatory network, we analysed a larger dataset of patient
372 SHH-MB.[33] Initial analysis of the data showed upregulation of all the aforementioned genes
373 in malignant cells compared to the non-malignant microenvironment (Fig. 4B). By contrast,
374 co-expression of these genes was weaker in other MB subtypes (Supplementary Fig. S5B).
375 Clustering the individual SHH-MB tumours showed that in 7/8 samples two to four clusters
376 emerged per tumour. One or more of these clusters expressed a *SOX2* regulatory network
377 that was highly similar to the regulatory network in DAOY cells in co-culture (Fig. 4C, D;
378 Supplementary Fig. S5C – H). The proportion of malignant cells expressing this signature
379 ranged from 4.2% to 20.3% (median 8.8%) in this dataset.[33] Quantification of the gene
380 signature across MB subtypes showed enrichment in SHH-MB tumours (Fig. 4E).
381 Furthermore, *TP53* mutation status (n = 2 *TP53* mutant SHH-MB tumours) was unrelated to
382 the occurrence of the gene signature. These data confirmed that the patterns of gene
383 expression in DAOY cells in co-culture were not simply an artifact related to our culture
384 conditions, and instead suggested DAOY cells mirrored a CSC-like state found *in vivo*.
385
386 **Greater transcriptional similarity of DAOY and ONS-76 cells in co-culture to patient SHH-**
387 **MB**
388 Encouraged by the transcriptional evidence suggesting tumour heterogeneity resembling
389 SHH-MB *in vivo* in our organoid co-culture model, we assessed the transcriptional similarity
390 of our model to patient tumours and PDX models. Therefore, we compared the
391 computational integration of DAOY and ONS-76 tumour cells in co-culture and PDX models
392 with patient SHH-MB tumours. We did not use canonical correlation implemented in Seurat
393 for this part of the analysis because this algorithm excessively blends distinct cancer cell
394 states.[21] Instead, we employed the fastMNN algorithm,[42] which performed well in an earlier
395 benchmarking study of tumour datasets [21] to integrate three public SHH-MB patient single-

396 cell datasets.[32] Upon projection in UMAP space two major clusters emerged to which all
397 three tumours contributed (Fig. 5A). Two SHH-MB PDX tumours [32] blended well with the
398 patient tumours but showed greater mixing with one of the two major clusters, suggesting
399 these PDX models did not recapitulate the full extent of transcriptional diversity of the
400 patient tumours (Fig. 5B, C). Whereas DAOY and ONS-76 cells in co-culture, as expected,
401 were less similar to patient tumours (Fig. 5D, E), in comparison with tumour spheroids of
402 either cell line far greater similarity was evident (Fig. 5F, G). We also computed a 'mixing
403 metric' to quantify how similar these datasets were after integration (Fig. 5H and
404 Supplementary Table 8).[43] Patient tumours scored the highest on this metric, followed
405 closely by PDX tumours. Strikingly, our tumour spheroid organoid co-culture models also
406 performed well, in contrast to tumour spheroid models.
407
408 **Discussion**
409 Human cerebellar organoid-based *in vitro* models have the potential to recapitulate patient
410 MB more faithfully compared to conventional *in vitro* models.[44] Here, we tested the
411 importance of the non-malignant microenvironment in regulating malignant cell states by
412 comparing the phenotypes of two long-established SHH-MB lines grown in co-culture or
413 conventionally. Compared to conventional *in vitro* models, we detected greater maturity of
414 malignant cells in co-culture. In particular, a subpopulation of ONS-76 cells activated the
415 expression of *NEUROD1*, a canonical marker of granule cells, only upon co-culture.
416 Additionally, a subpopulation of DAOY cells in co-culture expressed CSC-like markers and
417 pseudotime and functional enrichment analyses were concordant attesting to their capacity
418 for maturation into cells with neuronal features. The expression of CSC-like markers and
419 upregulation of neuronal differentiation genes by malignant cells in co-culture revealed the
420 emergence of cell states that were not observed in tumour cells cultured in isolation, under
421 our conditions. Given that similar cell states are found in mouse models, PDX models and
422 upon patient tumour molecular profiling,[6,32,40,45] we further demonstrated the convergence
423 of two SHH-MB cell lines towards *in vivo* cellular phenotypes. Therefore, the
424 microenvironment can non-cell autonomously regulate SHH-MB cell states. Moreover, our
425 computational analysis effectively addresses the challenge of the high non-malignant to
426 malignant cell ratio in our co-cultures. The resilience of Seurat to cell downsampling made
427 the identification of patient tumour-relevant cell states in our co-culture model possible.[12]

428

429 Given that malignant cell phenotypes in tumour spheroid-organoid co-culture were similar
430 to those seen *in vivo* in patient tumours and PDX models (Fig. 1D, E; Fig. 3B; Fig. 4; Fig. 5)
431 confirms the validity of our model in recapitulating patient tumours better than
432 conventional *in vitro* models. Moreover, our findings suggest that the consensus view that
433 these cell lines are poorly representative of patient tumours does not hold true when these
434 malignant cell lines are cultured in a more physiological context. The emergence of new cell
435 states in these long-established SHH-MB cell lines that was not evident in monolayer or
436 tumour spheroid culture conditions was striking, more so given the relatively short duration
437 (25 days) of co-culture. The immediate cause of these rapid phenotypic changes is likely to
438 be transcriptional plasticity, reflecting functional intra-tumour heterogeneity that is shared
439 by diverse malignant tumours.[46]
440

441 Malignant granule cells can differentiate in patient SHH-MB and in mouse models of this
442 disease.[32,33,45,47,48] Interestingly, the activation of *NEUROD1* in SHH-MB patient samples
443 showed no dependency on *TP53* mutational status (Supplementary Fig. S4D), suggesting
444 that differentiation processes can still be initiated in the presence of somatic *TP53*
445 mutations.[49] *NEUROD1* was upregulated in a sub-population of ONS-76 cells in tumour
446 spheroids in co-culture with organoids compared to tumour monocultures (Fig. 1D, E). In
447 both healthy and malignant cells, expression of *NEUROD1* was associated with actively
448 cycling cells and cells with neuronal features (Fig. 1G, I; Supplementary Fig. S3C – F).
449 Interestingly, however, in the malignant sub-population, upregulation of *NEUROD1* was not
450 as tightly coupled with neuronal differentiation compared to non-malignant granule cells.
451 These differences could reflect divergence of the properties of ONS-76 cells over an
452 extended period *in vitro*, favouring the survival of cycling cells over more differentiated
453 cells. Recent analysis of human granule cell ontogeny has demonstrated that, in contrast to
454 mouse, these cells express *NEUROD1* during their cycling phase.[31] The expression of this
455 gene in a smaller proportion of non-malignant cycling granule precursors is consistent with
456 the latter finding and further validates our cerebellar organoid model.
457

458 Our analysis showed that the DAOY CSC-like cells present in co-culture were enriched for
459 pathways related to the cell cycle, which suggested they were proliferative (Fig. 3G and

460 Supplementary Fig. S3C). Moreover, closely similar or equivalent cell states as defined by
461 expression of the *SOX2* regulatory network were present in a majority of samples across two
462 published scRNA-seq datasets that spanned infant to adult subtypes (Fig. 4 and
463 Supplementary Fig. S5C – H).[32,33] Reasons for the differences in the expressed members of
464 the *SOX2* regulatory network in CSC-like subpopulations are unclear. Differences could
465 relate to redundancy of distinct *SOX2* regulators or reflect divergence of functional states
466 within CSC-like populations, associated with, for example, different proliferation rates and
467 sensitivity to therapy. The traditional view is that CSC are rare, slow-cycling cells that are
468 relatively quiescent compared to other malignant cells, and such tumour-initiating cells
469 were identified in a SHH-MB mouse model.[6,40] The proportion of CSC-like cells in the scRNA-
470 seq dataset we analysed [33] was up to ~20% with a median close to 10%, suggesting these
471 cells might be more common than previously thought. Moreover, in another brain tumour,
472 glioma, stem cells have also been reported to be proliferative, supporting the view that CSC
473 states are non-uniform.[4] Future functional studies are needed to determine if the SHH-MB
474 cells with the signature we identified meet the standard for stemness in *in vivo* limiting
475 dilution assays. Pseudotime and functional enrichment analyses were consistent and
476 suggested these cells underwent a maturation process, associated with a continuum of cell
477 states that led to the acquisition of neuron-like features (Fig. 3F – H). Furthermore, we
478 discounted the possibility that the emergence of a CSC-like state in DAOY cells was caused
479 by the *TP53* mutation because of the prevalence of a CSC-like state in patient SHH-MB
480 analysed here that were wild type for *TP53* and the expression of NSC markers in ONS-76
481 cells in tumour spheroid-organoid co-culture (Fig. 2E).
482
483 In our co-culture model, single or multiple constituents of the non-malignant
484 microenvironment could induce the emergent phenotypic states of SHH-MB cells.
485 Regulatory interactions between malignant and non-malignant components that exploit
486 local signalling networks are a well-established mechanism for tumour cells to gain a growth
487 advantage.[50] Microenvironmental factors implicated in these signalling networks *in vivo*
488 include stromal cells, blood and lymphatic vessels, immune-inflammatory cells and
489 extracellular matrix (ECM). Of these, ECM is the only one of these factors represented in our
490 co-culture model and has a well-recognised role in tumour progression.[51] Whether other
491 components of the microenvironment in our model, namely progenitors, neurons, glia, roof

plate or choroid plexus can produce malignant cell state-reprogramming signals is unclear. Identification of this factor(s) in future could open new therapeutic options.

Funding

This work was supported by Cancer Research UK (CRUK) grant number C2195/A28699, through a CRUK Oxford Centre Clinical Research Training Fellowship to MvE and by a Medical Research Council award to JJ (award number: MR/V037730/1). BSB is funded by the Ludwig Institute for Cancer Research.

Conflicts of Interest

The authors declare they have no conflict of interest.

Authorship

JJ conceived the project and JJ and MvE designed experiments. MvE performed the experimental work and AN and JJ performed data analysis. EB and BSB provided advice on experimental design and analysis. JJ wrote the manuscript with contributions from all the authors.

Data Availability

scRNA-seq data have been deposited in the National Centre for Biotechnology Information Gene Expression Omnibus (GEO) database and are publicly accessible through GEO accession number GSE254917 (https://www.ncbi.nlm.nih.gov/geo/query/acc.cgi?acc=GSE254917). Analysis code is available at https://github.com/jjacob12/carp_analysis50K/tree/main/PrePrint.

Acknowledgements

Computation used the Oxford Biomedical Research Computing (BMRC) facility, a joint development between the Wellcome Centre for Human Genetics and the Big Data Institute supported by Health Data Research UK and the NIHR Oxford Biomedical Research Centre. We thank Dr Jia-Ling Ruan (Department of Oncology, Medical Sciences Division, University of Oxford) for preparing SHH-MB cell lines for authentication.

524 **Figure Legends**

525 **Figure 1**. Upregulation of *NEUROD1* in ONS-76 cells in co-culture compared to monolayer or
526 tumour spheroid growth conditions. (A) Schematic of experimental workflow. This figure
527 was created with BioRender.com. (B) UMAP visualisation of single-cell transcriptomes of
528 ONS-76 cells in co-culture identified two malignant cell clusters annotated as
529 'ONS76_cluster_3' and 'ONS76_cluster_10'. (C) Violin plot showing co-expression of
530 *NEUROD1*, *RTN1* and *RBFOX3* in the 'Granule neurons' cluster of the control organoid. (D)
531 Violin plot of expression of *NEUROD1,* and absent *RTN1* and *RBFOX3* expression in
532 'ONS76_cluster_3' in the ONS-76 tumour spheroid-organoid co-culture (E) Violin plots of the
533 expression of *NEUROD1* in ONS-76 cells (upper panel) and DAOY cells (lower panel) grown
534 as monolayers, tumour spheroids or in tumour spheroid-organoid co-culture. (F) Expression
535 of *NEUROD1* in the DAOY tumour spheroid-organoid co-culture sample is restricted to the
536 non-malignant 'Granule neurons' cluster. (G) fgsea gene set enrichment of upregulated gene
537 ontology (GO) biological pathway terms evaluated by normalised enrichment scores of the
538 *NEUROD1*+ cluster of malignant cells ('ONS76_cluster_3') in the ONS-76 tumour spheroid-
539 organoid co-culture sample. (H) Violin plot of marker genes of the second malignant cluster,
540 'ONS76_cluster_10' in the ONS-76 tumour spheroid-organoid co-culture sample. (I) fgsea
541 gene set enrichment of upregulated GO biological pathway terms evaluated by normalised
542 enrichment scores of non-malignant *NEUROD1*+ cells ('Granule neurons') in the ONS-76
543 tumour spheroid-organoid co-culture sample.

544

545 **Figure 2**. Upregulation of neural stem cell markers in DAOY malignant cells in co-culture. (A)
546 UMAP visualisation of single-cell transcriptomes in DAOY tumour spheroid-organoid co-
547 cultures shows three malignant clusters annotated as 'DAOY_cluster_9, 'DAOY_cluster_13'
548 and 'DAOY_cluster_14'. (B) Violin plots showing expression of unique markers of malignant
549 DAOY clusters in co-culture. (C) Violin plots of expression of the indicated neural stem cell
550 markers in DAOY cells in tumour spheroid-organoid co-culture, tumour spheroid and
551 monolayer cultures. (D) Expression of the indicated genes in cells of the control organoid
552 sample. (E) Violin plots of expression of the indicated neural stem cell markers in ONS-76
553 cells in tumour spheroid-organoid co-culture, tumour spheroid and monolayer cultures.

554

555 **Figure 3**. Multiple factors known to regulate the expression of *SOX2* in NSC and ES cells (ESC)
556 are also expressed in a sub-population of DAOY cells in co-culture. (A) Schematic of the
557 *SOX2* regulatory network in NSC and ESC (adapted from Bertolini et al.[41]). (B) Violin plots of
558 expression of the *SOX2* regulatory network in 'DAOY_cluster_9' cells. (C) Expression of a
559 sparse *SOX2* regulatory network in ONS-76 cells in tumour spheroid-organoid co-culture. (D)
560 *SOX2* regulatory network expression in DAOY and ONS-76 monolayer and tumour spheroid
561 cultures. (E) Gene expression of the *SOX2* regulatory network in non-malignant organoids.
562 (F) Pseudotime trajectory of cells in 'DAOY_cluster_9'. (G) Enrichment of GO biological
563 pathway terms upregulated in 'DAOY_cluster_9' visualised in Cytoscape.[18] (H) Enrichment of
564 GO biological pathway terms upregulated in 'DAOY_cluster_13' visualised in Cytoscape. (I)
565 Enrichment of GO biological pathway terms upregulated in 'DAOY_cluster_10' visualised in
566 Cytoscape. *TBX6* was not expressed in malignant cells.
567
568 **Figure 4**.
569 Expression of the *SOX2* regulatory network in patient SHH-MB datasets sequenced at single-
570 cell level. (A) Violin plots of the expression of the *SOX2* regulatory network in one of three
571 patient SHH-MB (tumour ID: SJ454) and in a SHH-MB PDX tumour model (tumour ID:
572 RMCB18) from the same dataset.[32] (B) Heatmap of expression of the *SOX2* regulatory
573 network in malignant cells and in cells of the microenvironment in a second patient SHH-MB
574 dataset.[33] Cell labels are retained from the original publication. (C) Expression of the *SOX2*
575 regulatory network in two of three UMAP clusters in a patient tumour (tumour ID: 1235)
576 from the same dataset.[33] (D) *SOX2* regulatory network expression in another tumour
577 (tumour ID: 801) from the same dataset.[33] (E) Violin plots of cell scores for the *SOX2*
578 regulatory network in all medulloblastoma subtypes. Only malignant cells are included.[33] For
579 malignant cell numbers in each SHH-MB see Supplementary Fig. S4. *TBX6* was not expressed
580 in malignant cells in either dataset.
581
582 **Figure 5**. The co-culture tumour models recapitulate SHH-MB patient tumours better than
583 conventional *in vitro* models. (A) UMAP visualisation of three SHH-MB patient tumours. (B)
584 Integration and UMAP visualisation of cells from a PDX SHH-MB tumour (PDX1) with the
585 same three SHH-MB patient tumours as in A. (C) Integration and UMAP visualisation of cells
586 from a second PDX SHH-MB tumour (PDX2) with the three SHH-MB patient tumours. (D)

587 Integration and UMAP visualisation of DAOY cells in tumour spheroid-organoid co-culture
588 with the three SHH-MB patient tumours. (E) Integration and UMAP visualisation of ONS-76
589 cells in tumour spheroid-organoid co-culture with the three patient SHH-MB tumours. (F)
590 Integration and UMAP visualisation of DAOY tumour spheroid cells with the three patient
591 SHH-MB tumours. (G) Integration and UMAP visualisation of ONS-76 tumour spheroid cells
592 with the three patient SHH-MB tumours. (H) Violin plots of mixing metric scores of the
593 integrations shown in A to G. Patient and PDX tumour datasets were obtained from the
594 published study by Hovestadt et al.[32] Only malignant cells were used for scoring.
595
596
597
598 **References**
599

600 **1.** Dolecek TA, Propp JM, Stroup NE, Kruchko C. CBTRUS statistical report: primary brain
601 and central nervous system tumors diagnosed in the United States in 2005-2009.
602 *Neuro Oncol.* 2012; 14 Suppl 5(Suppl 5):v1-49.
603 **2.** Garcia-Lopez J, Kumar R, Smith KS, Northcott PA. Deconstructing Sonic Hedgehog
604 Medulloblastoma: Molecular Subtypes, Drivers, and Beyond. *Trends Genet.* 2021;
605 37(3):235-250.
606 **3.** Wechsler-Reya RJ, Scott MP. Control of neuronal precursor proliferation in the
607 cerebellum by Sonic Hedgehog. *Neuron.* 1999; 22(1):103-114.
608 **4.** Gimple RC, Yang K, Halbert ME, Agnihotri S, Rich JN. Brain cancer stem cells:
609 resilience through adaptive plasticity and hierarchical heterogeneity. *Nat Rev Cancer.*
610 2022; 22(9):497-514.
611 **5.** Hagey DW, Klum S, Kurtsdotter I, Zaouter C, Topcic D, Andersson O, Bergsland M,
612 Muhr J. SOX2 regulates common and specific stem cell features in the CNS and
613 endoderm derived organs. *PLoS Genet.* 2018; 14(2):e1007224.
614 **6.** Selvadurai HJ, Luis E, Desai K, Lan X, Vladoiu MC, Whitley O, Galvin C, Vanner RJ, Lee
615 L, Whetstone H, Kushida M, Nowakowski T, Diamandis P, Hawkins C, Bader G,
616 Kriegstein A, Taylor MD, Dirks PB. Medulloblastoma Arises from the Persistence of a
617 Rare and Transient Sox2(+) Granule Neuron Precursor. *Cell Rep.* 2020; 31(2):107511.
618 **7.** Ivanov DP, Coyle B, Walker DA, Grabowska AM. In vitro models of medulloblastoma:
619 Choosing the right tool for the job. *Journal of Biotechnology.* 2016; 236:10-25.
620 **8.** van Essen MJ, Apsley EJ, Riepsaame J, Xu R, Northcott PA, Cowley SA, Jacob J, Becker
621 EBE. PTCH1-mutant human cerebellar organoids exhibit altered neural development
622 and recapitulate early medulloblastoma tumorigenesis. *Dis Model Mech.* 2024; 17(2).
623 **9.** van Essen MJ, Nayler S, Apsley EJ, Jacob J, Becker EBE. Cerebellar Modelling Using
624 Human Induced Pluripotent Stem Cells (hiPSCs). In: Sillitoe RV, ed. *Measuring*
625 *Cerebellar Function*. New York, NY: Springer US; 2022:1-21.
626 **10.** Handel AE, Chintawar S, Lalic T, Whiteley E, Vowles J, Giustacchini A, Argoud K, Sopp
627 P, Nakanishi M, Bowden R, Cowley S, Newey S, Akerman C, Ponting CP, Cader MZ.

628 Assessing similarity to primary tissue and cortical layer identity in induced
629 pluripotent stem cell-derived cortical neurons through single-cell transcriptomics.
630 *Human Molecular Genetics.* 2016; 25(5):989-1000.
631 **11.** Osorio D, Cai JJ. Systematic determination of the mitochondrial proportion in human
632 and mice tissues for single-cell RNA-sequencing data quality control. *Bioinformatics.*
633 2021; 37(7):963-967.
634 **12.** Joseph MR, Lambda M, Pétur Helgi E, Kayla J, Laura L, Booeshaghi AS, Sindri A,
635 Delaney KS, Nicolas B, Páll M, Lior P. The impact of package selection and versioning
636 on single-cell RNA-seq analysis. *bioRxiv.* 2024:2024.2004.2004.588111.
637 **13.** Hao Y, Hao S, Andersen-Nissen E, Mauck WM, 3rd, Zheng S, Butler A, Lee MJ, Wilk AJ,
638 Darby C, Zager M, Hoffman P, Stoeckius M, Papalexi E, Mimitou EP, Jain J, Srivastava
639 A, Stuart T, Fleming LM, Yeung B, Rogers AJ, McElrath JM, Blish CA, Gottardo R,
640 Smibert P, Satija R. Integrated analysis of multimodal single-cell data. *Cell.* 2021;
641 184(13):3573-3587 e3529.
642 **14.** Korsunsky I, Nathan A, Millard N, Raychaudhuri S. Presto scales Wilcoxon and auROC
643 analyses to millions of observations. *bioRxiv.* 2019:653253.
644 **15.** Liberzon A, Birger C, Thorvaldsdóttir H, Ghandi M, Mesirov JP, Tamayo P. The
645 Molecular Signatures Database (MSigDB) hallmark gene set collection. *Cell Syst.*
646 2015; 1(6):417-425.
647 **16.** Sergushichev AA. An algorithm for fast preranked gene set enrichment analysis using
648 cumulative statistic calculation. *bioRxiv.* 2016:060012.
649 **17.** Kolberg L, Raudvere U, Kuzmin I, Adler P, Vilo J, Peterson H. g:Profiler—interoperable
650 web service for functional enrichment analysis and gene identifier mapping (2023
651 update). *Nucleic Acids Research.* 2023; 51(W1):W207-W212.
652 **18.** Shannon P, Markiel A, Ozier O, Baliga NS, Wang JT, Ramage D, Amin N, Schwikowski
653 B, Ideker T. Cytoscape: a software environment for integrated models of
654 biomolecular interaction networks. *Genome Res.* 2003; 13(11):2498-2504.
655 **19.** Cao J, Spielmann M, Qiu X, Huang X, Ibrahim DM, Hill AJ, Zhang F, Mundlos S,
656 Christiansen L, Steemers FJ, Trapnell C, Shendure J. The single-cell transcriptional
657 landscape of mammalian organogenesis. *Nature.* 2019; 566(7745):496-502.
658 **20.** Haghverdi L, Lun ATL, Morgan MD, Marioni JC. Batch effects in single-cell RNA-
659 sequencing data are corrected by matching mutual nearest neighbors. *Nat*
660 *Biotechnol.* 2018; 36(5):421-427.
661 **21.** Laura MR, Mazdak R, Suluxan M, Shamini A, Danielle CC, Díaz-Mejía JJ, Fiona JC,
662 Peter BD, Trevor JP. A comparison of data integration methods for single-cell RNA
663 sequencing of cancer samples. *bioRxiv.* 2021:2021.2008.2004.453579.
664 **22.** Schäfer M, Werner S. Cancer as an overhealing wound: an old hypothesis revisited.
665 *Nat Rev Mol Cell Biol.* 2008; 9(8):628-638.
666 **23.** Nguyen LXT, Raval A, Garcia JS, Mitchell BS. Regulation of Ribosomal Gene
667 Expression in Cancer. *Journal of Cellular Physiology.* 2015; 230(6):1181-1188.
668 **24.** Janiszewska M, Primi MC, Izard T. Cell adhesion in cancer: Beyond the migration of
669 single cells. *J Biol Chem.* 2020; 295(8):2495-2505.
670 **25.** Owa T, Taya S, Miyashita S, Yamashita M, Adachi T, Yamada K, Yokoyama M, Aida S,
671 Nishioka T, Inoue YU, Goitsuka R, Nakamura T, Inoue T, Kaibuchi K, Hoshino M.
672 Meis1 Coordinates Cerebellar Granule Cell Development by Regulating Pax6
673 Transcription, BMP Signaling and Atoh1 Degradation. *J Neurosci.* 2018; 38(5):1277-
674 1294.

675 **26.** Machold R, Klein C, Fishell G. Genes expressed in Atoh1 neuronal lineages arising
676 from the r1/isthmus rhombic lip. *Gene Expr Patterns.* 2011; 11(5-6):349-359.
677 **27.** Xu X, Stoyanova EI, Lemiesz AE, Xing J, Mash DC, Heintz N. Species and cell-type
678 properties of classically defined human and rodent neurons and glia. *Elife.* 2018; 7.
679 **28.** Bizzoca A, Virgintino D, Lorusso L, Buttiglione M, Yoshida L, Polizzi A, Tattoli M,
680 Cagiano R, Rossi F, Kozlov S, Furley A, Gennarini G. Transgenic mice expressing
681 F3/contactin from the TAG-1 promoter exhibit developmentally regulated changes in
682 the differentiation of cerebellar neurons. *Development.* 2003; 130(1):29-43.
683 **29.** Nayler S, Agarwal D, Curion F, Bowden R, Becker EBE. High-resolution transcriptional
684 landscape of xeno-free human induced pluripotent stem cell-derived cerebellar
685 organoids. *Scientific Reports.* 2021; 11(1):12959.
686 **30.** Miyata T, Maeda T, Lee JE. NeuroD is required for differentiation of the granule cells
687 in the cerebellum and hippocampus. *Genes Dev.* 1999; 13(13):1647-1652.
688 **31.** Behesti H, Kocabas A, Buchholz DE, Carroll TS, Hatten ME. Altered temporal
689 sequence of transcriptional regulators in the generation of human cerebellar granule
690 cells. *eLife.* 2021; 10:e67074.
691 **32.** Hovestadt V, Smith KS, Bihannic L, Filbin MG, Shaw ML, Baumgartner A, DeWitt JC,
692 Groves A, Mayr L, Weisman HR, Richman AR, Shore ME, Goumnerova L, Rosencrance
693 C, Carter RA, Phoenix TN, Hadley JL, Tong Y, Houston J, Ashmun RA, DeCuypere M,
694 Sharma T, Flasch D, Silkov A, Ligon KL, Pomeroy SL, Rivera MN, Rozenblatt-Rosen O,
695 Rusert JM, Wechsler-Reya RJ, Li X-N, Peyrl A, Gojo J, Kirchhofer D, Lötsch D, Czech T,
696 Dorfer C, Haberler C, Geyeregger R, Halfmann A, Gawad C, Easton J, Pfister SM,
697 Regev A, Gajjar A, Orr BA, Slavc I, Robinson GW, Bernstein BE, Suvà ML, Northcott
698 PA. Resolving medulloblastoma cellular architecture by single-cell genomics. *Nature.*
699 2019; 572(7767):74-79.
700 **33.** Riemondy KA, Venkataraman S, Willard N, Nellan A, Sanford B, Griesinger AM, Amani
701 V, Mitra S, Hankinson TC, Handler MH, Sill M, Ocasio J, Weir SJ, Malawsky DS,
702 Gershon TR, Garancher A, Wechsler-Reya RJ, Hesselberth JR, Foreman NK, Donson
703 AM, Vibhakar R. Neoplastic and immune single-cell transcriptomics define subgroup-
704 specific intra-tumoral heterogeneity of childhood medulloblastoma. *Neuro Oncol.*
705 2022; 24(2):273-286.
706 **34.** Brotto DB, Siena ÁDD, de Barros II, Carvalho SdCeS, Muys BR, Goedert L, Cardoso C,
707 Plaça JR, Ramão A, Squire JA, Araujo LF, Silva WAd. Contributions of HOX genes to
708 cancer hallmarks: Enrichment pathway analysis and review. *Tumor Biology.* 2020;
709 42(5):1010428320918050.
710 **35.** Zhang H, Zheng J, Fu Y, Ling J, Liu Z, Lin X, Dong X, Sun Y, Tan T, Guo Z, Xie G.
711 Overexpression of POU3F2 promotes radioresistance in triple-negative breast cancer
712 via Akt pathway activation. *Breast Cancer Research and Treatment.* 2023;
713 198(3):437-446.
714 **36.** Tomoo O, Shinichiro T, Satoshi M, Mariko Y, Toma A, Koyo Y, Miwa Y, Shogo A,
715 Tomoki N, Yukiko UI, Ryo G, Takuro N, Takayoshi I, Kozo K, Mikio H. Meis1
716 Coordinates Cerebellar Granule Cell Development by Regulating Pax6 Transcription,
717 BMP Signaling and Atoh1 Degradation. *The Journal of Neuroscience.* 2018;
718 38(5):1277.
719 **37.** Shao W, Ding Q, Guo Y, Xing J, Huo Z, Wang Z, Xu Q, Guo Y. A Pan-Cancer Landscape
720 of HOX-Related lncRNAs and Their Association With Prognosis and Tumor
721 Microenvironment. *Front Mol Biosci.* 2021; 8:767856.

722 **38.** Tantin D. Oct transcription factors in development and stem cells: insights and
723 mechanisms. *Development.* 2013; 140(14):2857-2866.
724 **39.** Yuzwa SA, Borrett MJ, Innes BT, Voronova A, Ketela T, Kaplan DR, Bader GD, Miller
725 FD. Developmental Emergence of Adult Neural Stem Cells as Revealed by Single-Cell
726 Transcriptional Profiling. *Cell Reports.* 2017; 21(13):3970-3986.
727 **40.** Vanner RJ, Remke M, Gallo M, Selvadurai HJ, Coutinho F, Lee L, Kushida M, Head R,
728 Morrissy S, Zhu X, Aviv T, Voisin V, Clarke ID, Li Y, Mungall AJ, Moore RA, Ma Y, Jones
729 SJ, Marra MA, Malkin D, Northcott PA, Kool M, Pfister SM, Bader G, Hochedlinger K,
730 Korshunov A, Taylor MD, Dirks PB. Quiescent sox2(+) cells drive hierarchical growth
731 and relapse in sonic hedgehog subgroup medulloblastoma. *Cancer Cell.* 2014;
732 26(1):33-47.
733 **41.** Bertolini J, Mercurio S, Favaro R, Mariani J, Ottolenghi S, Nicolis SK. Sox2-Dependent
734 Regulation of Neural Stem Cells and CNS Development. In: Kondoh H, Lovell-Badge R,
735 eds. *Sox2: Biology and Role in Development and Disease*: Academic Press; 2016:187-
736 216.
737 **42.** Lun ATL. A description of the theory behind the fastMNN algorithm. 2019;
738 https://marionilab.github.io/FurtherMNN2018/theory/description.html.
739 **43.** Stuart T, Butler A, Hoffman P, Hafemeister C, Papalexi E, Mauck WM, 3rd, Hao Y,
740 Stoeckius M, Smibert P, Satija R. Comprehensive Integration of Single-Cell Data. *Cell.*
741 2019; 177(7):1888-1902 e1821.
742 **44.** Essen MJv, Riepsaame J, Cowley SA, Jacob J, Becker EBE. PTCH1 mutant human
743 cerebellar organoids are associated with altered neural development and early
744 pathways of medulloblastoma oncogenesis. *bioRxiv.* 2023:2023.2005.2010.540200.
745 **45.** Vladoiu MC, El-Hamamy I, Donovan LK, Farooq H, Holgado BL, Sundaravadanam Y,
746 Ramaswamy V, Hendrikse LD, Kumar S, Mack SC, Lee JJY, Fong V, Juraschka K,
747 Przelicki D, Michealraj A, Skowron P, Luu B, Suzuki H, Morrissy AS, Cavalli FMG,
748 Garzia L, Daniels C, Wu X, Qazi MA, Singh SK, Chan JA, Marra MA, Malkin D, Dirks P,
749 Heisler L, Pugh T, Ng K, Notta F, Thompson EM, Kleinman CL, Joyner AL, Jabado N,
750 Stein L, Taylor MD. Childhood cerebellar tumours mirror conserved fetal
751 transcriptional programs. *Nature.* 2019; 572(7767):67-73.
752 **46.** Smith BA, Balanis NG, Nanjundiah A, Sheu KM, Tsai BL, Zhang Q, Park JW, Thompson
753 M, Huang J, Witte ON, Graeber TG. A Human Adult Stem Cell Signature Marks
754 Aggressive Variants across Epithelial Cancers. *Cell Rep.* 2018; 24(12):3353-
755 3366.e3355.
756 **47.** Cheng Y, Liao S, Xu G, Hu J, Guo D, Du F, Contreras A, Cai KQ, Peri S, Wang Y, Corney
757 DC, Noronha AM, Chau LQ, Zhou G, Wiest DL, Bellacosa A, Wechsler-Reya RJ, Zhao Y,
758 Yang ZJ. NeuroD1 Dictates Tumor Cell Differentiation in Medulloblastoma. *Cell Rep.*
759 2020; 31(12):107782.
760 **48.** Ocasio JK, Babcock B, Malawsky D, Weir SJ, Loo L, Simon JM, Zylka MJ, Hwang D,
761 Dismuke T, Sokolsky M, Rosen EP, Vibhakar R, Zhang J, Saulnier O, Vladoiu M, El-
762 Hamamy I, Stein LD, Taylor MD, Smith KS, Northcott PA, Colaneri A, Wilhelmsen K,
763 Gershon TR. scRNA-seq in medulloblastoma shows cellular heterogeneity and
764 lineage expansion support resistance to SHH inhibitor therapy. *Nat Commun.* 2019;
765 10(1):5829.
766 **49.** Oh L, Hafsi H, Hainaut P, Ariffin H. p53, stem cell biology and childhood blastomas.
767 *Current Opinion in Oncology.* 2019; 31(2).

768 **50.** Wang M, Zhao J, Zhang L, Wei F, Lian Y, Wu Y, Gong Z, Zhang S, Zhou J, Cao K, Li X,
769 Xiong W, Li G, Zeng Z, Guo C. Role of tumor microenvironment in tumorigenesis.
770 *Journal of Cancer.* 2017; 8(5):761-773.
771 **51.** Pickup MW, Mouw JK, Weaver VM. The extracellular matrix modulates the hallmarks
772 of cancer. *EMBO Rep.* 2014; 15(12):1243-1253.
773

774

Figure 1

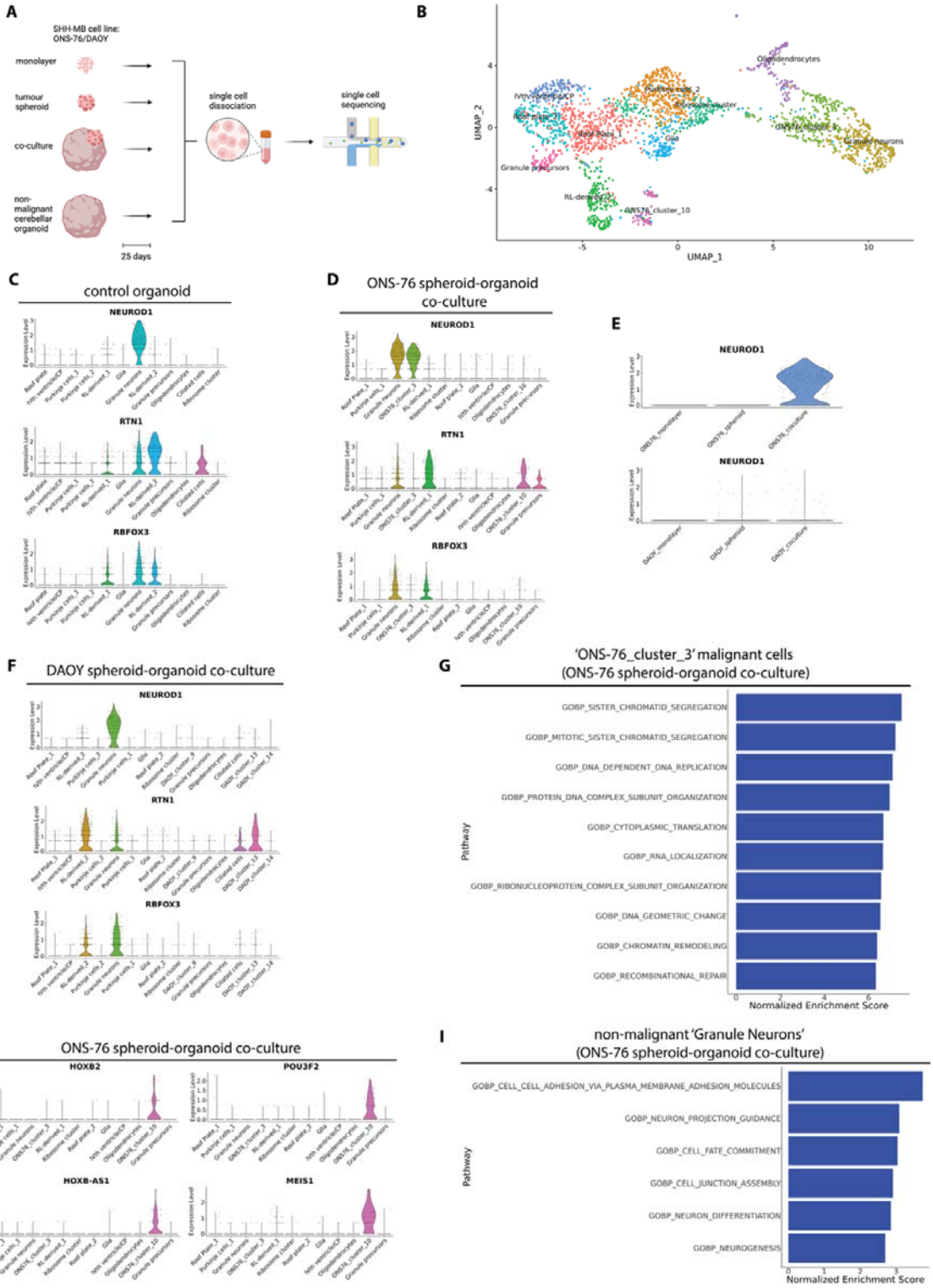
A
SHH-MB cell line: ONS-76/DAOY
monolayer
tumour spheroid
co-culture
non-malignant cerebellar organoid
25 days
single cell dissociation
single cell sequencing
B
UMAP_1
UMAP_2
Oligodendrocytes
Granule precursors
RL-derived_2
ONS76_cluster_10
C
control organoid
NEUROD1
RTN1
RBFOX3
D
ONS-76 spheroid-organoid co-culture
NEUROD1
RTN1
RBFOX3
E
NEUROD1
NEUROD1
F
DAOY spheroid-organoid co-culture
NEUROD1
RTN1
RBFOX3
G
'ONS-76_cluster_3' malignant cells
(ONS-76 spheroid-organoid co-culture)
GOBP_SISTER_CHROMATID_SEGREGATION
GOBP_MITOTIC_SISTER_CHROMATID_SEGREGATION
GOBP_DNA_DEPENDENT_DNA_REPLICATION
GOBP_PROTEIN_DNA_COMPLEX_SUBUNIT_ORGANIZATION
GOBP_CYTOPLASMIC_TRANSLATION
GOBP_RNA_LOCALIZATION
GOBP_RIBONUCLEOPROTEIN_COMPLEX_SUBUNIT_ORGANIZATION
GOBP_DNA_GEOMETRIC_CHANGE
GOBP_CHROMATIN_REMODELING
GOBP_RECOMBINATIONAL_REPAIR
Pathway
Normalized Enrichment Score
H
ONS-76 spheroid-organoid co-culture
HOXB2
POU3F2
HOXB-AS1
MEIS1
I
non-malignant 'Granule Neurons'
(ONS-76 spheroid-organoid co-culture)
GOBP_CELL_CELL_ADHESION_VIA_PLASMA_MEMBRANE_ADHESION_MOLECULES
GOBP_NEURON_PROJECTION_GUIDANCE
GOBP_CELL_FATE_COMMITMENT
GOBP_CELL_JUNCTION_ASSEMBLY
GOBP_NEURON_DIFFERENTIATION
GOBP_NEUROGENESIS
Pathway
Normalized Enrichment Score

Figure 2

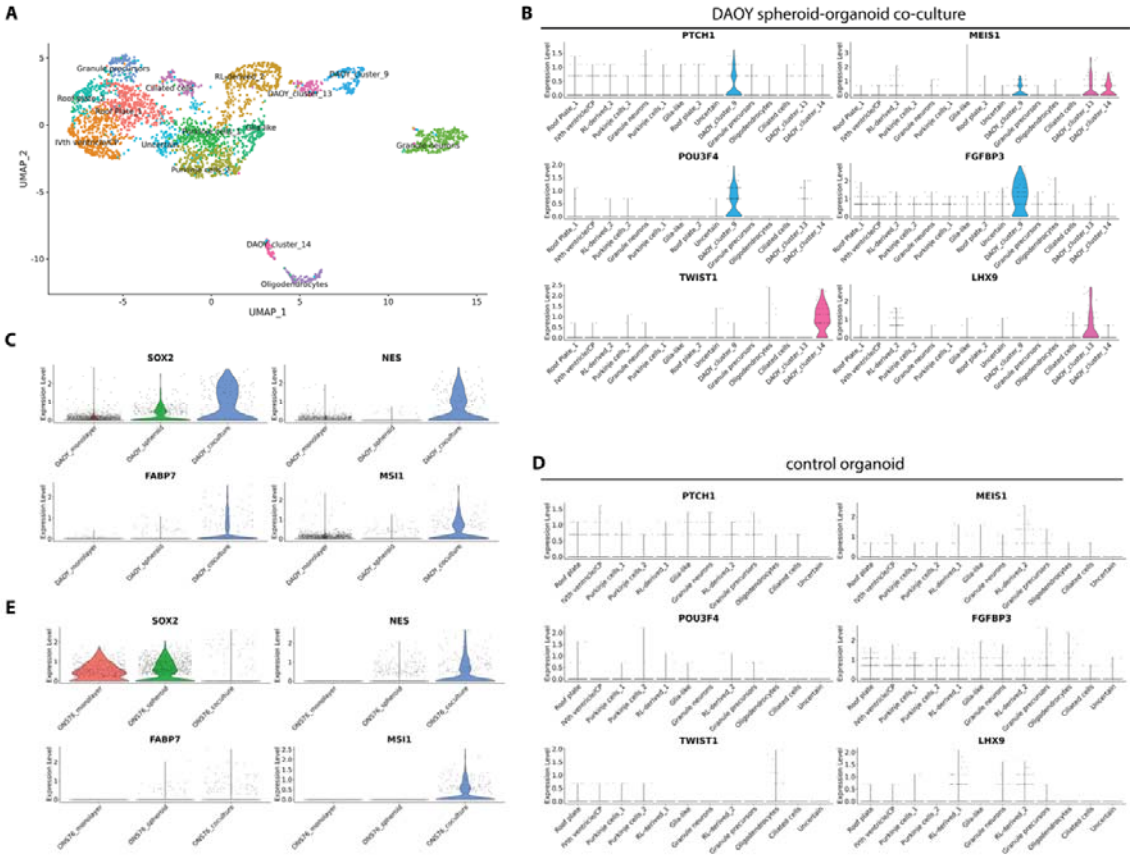
A
UMAP_1
UMAP_2
B
DAOY spheroid-organoid co-culture
PTCH1
MEIS1
POU3F4
FGFBP3
TWIST1
LHX9
C
SOX2
NES
FABP7
MSI1
D
control organoid
PTCH1
MEIS1
POU3F4
FGFBP3
TWIST1
LHX9
E
SOX2
NES
FABP7
MSI1

Figure 3

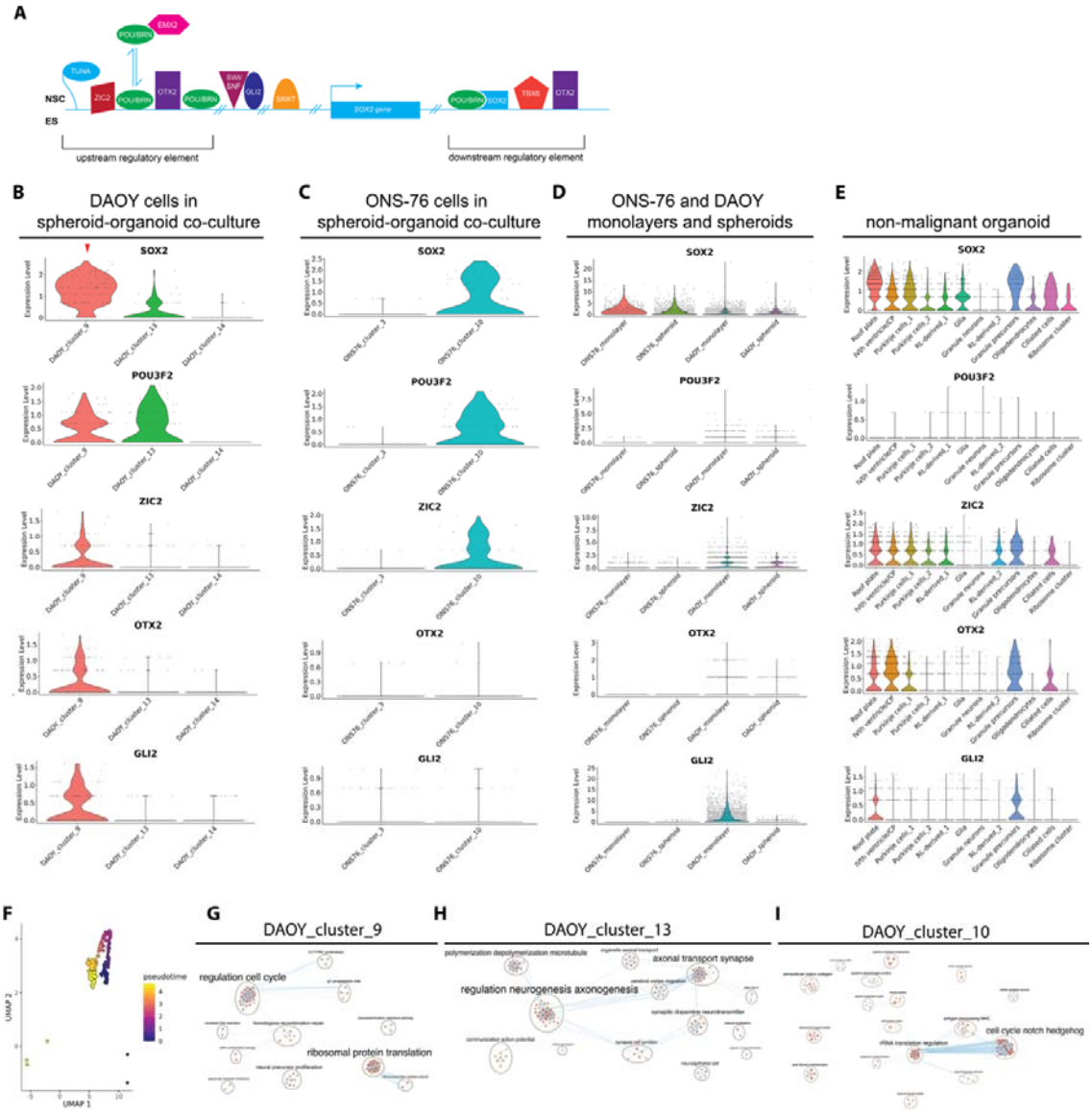

781

782

Figure 4

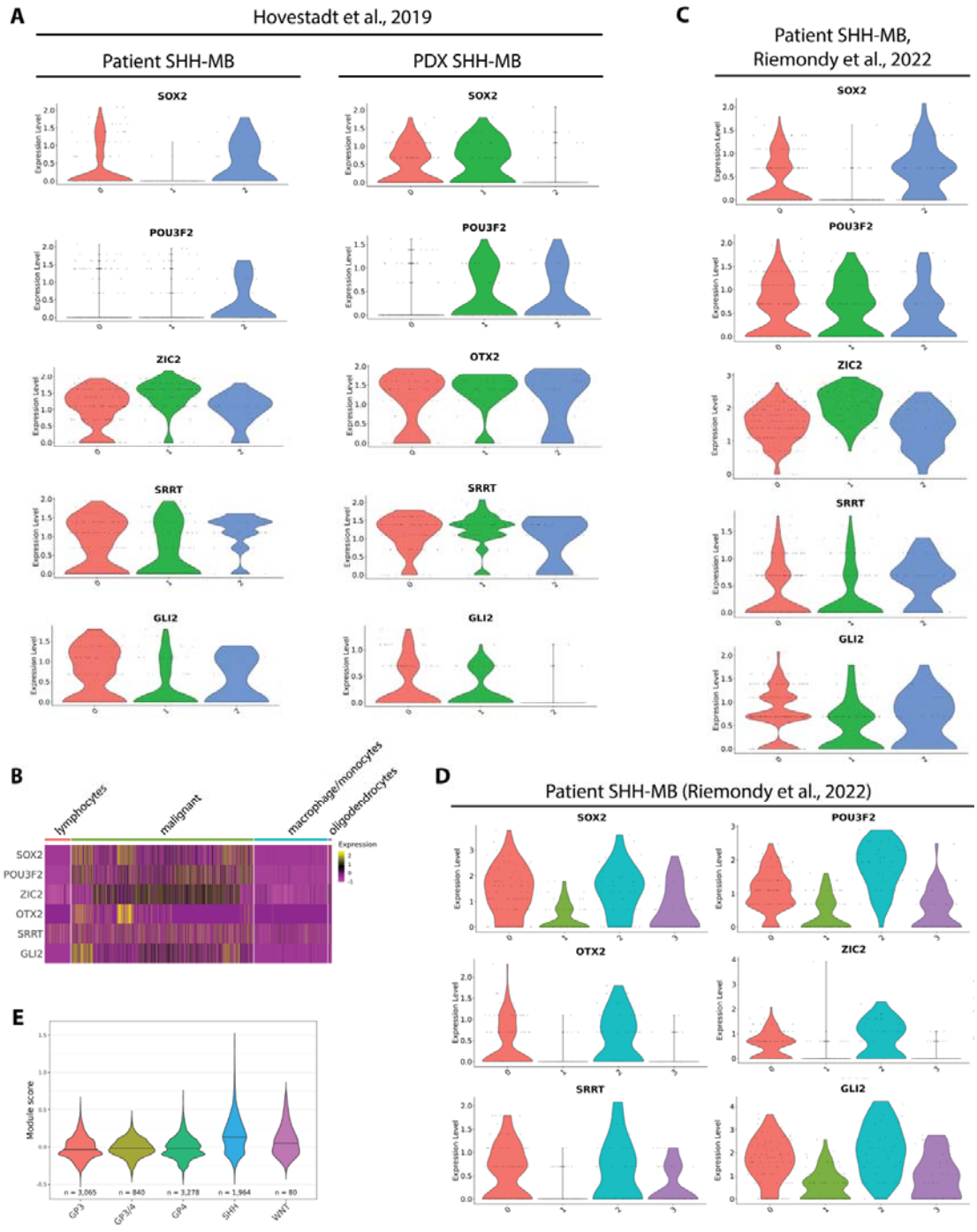

783

784

Figure 5

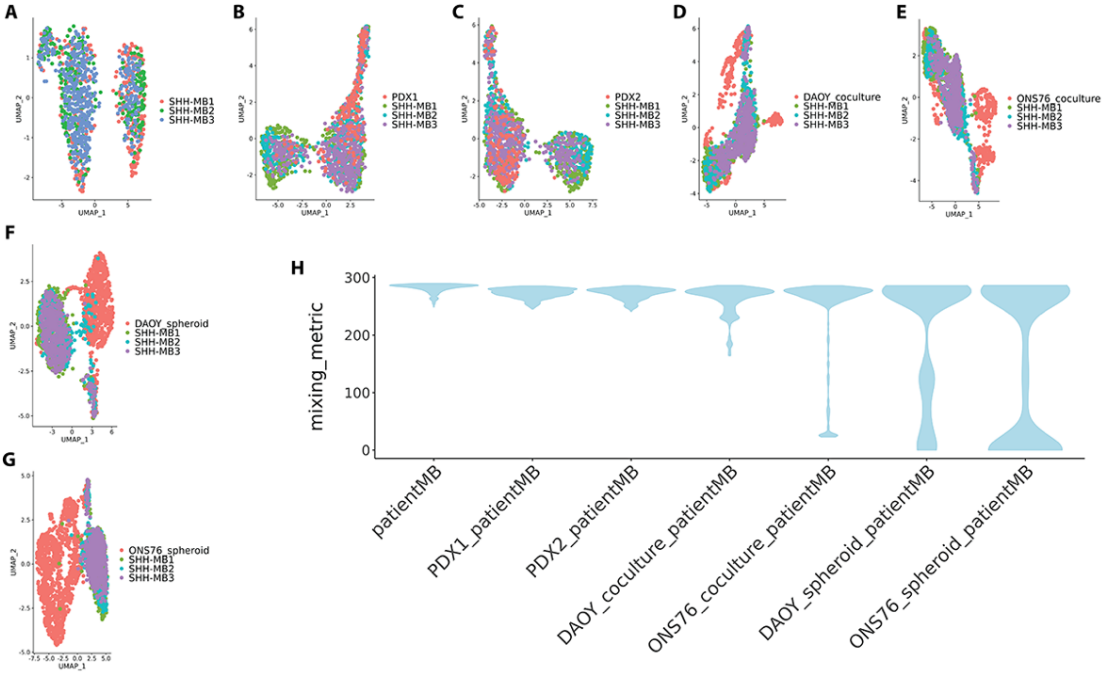
A
SHH-MB1
SHH-MB2
SHH-MB3
B
PDX1
SHH-MB1
SHH-MB2
SHH-MB3
C
PDX2
SHH-MB1
SHH-MB2
SHH-MB3
D
DAOY_coculture
SHH-MB1
SHH-MB2
SHH-MB3
E
ONS76_coculture
SHH-MB1
SHH-MB2
SHH-MB3
F
DAOY_spheroid
SHH-MB1
SHH-MB2
SHH-MB3
G
ONS76_spheroid
SHH-MB1
SHH-MB2
SHH-MB3
H
mixing_metric
300
200
100
0
patientMB
PDX1_patientMB
PDX2_patientMB
DAOY_coculture_patientMB
ONS76_coculture_patientMB
DAOY_spheroid_patientMB
ONS76_spheroid_patientMB